Hindawi
Advances in Civil Engineering
Volume 2023, Article ID 9916513, 18 pages
https://doi.org/10.1155/2023/9916513

Research Article

Study of the Roof Deformation Characteristics of Roadway Excavation Face and Unsupported Roof Distance

Jie Zhang,[1,2] Shoushi Gao,[1] Yifeng He,[1] Tao Yang,[1] Bing Wang,[1] Li Wang,[1] Haibo Pang,[1] and Bing Peng[3]

[1]*School of Energy Resources, Xi'an University of Science and Technology, Xian 710054, China*
[2]*Key Laboratory of Mine Mining and Disaster Prevention in West China, Ministry of Education, Xian 710054, China*
[3]*Shanxi Mineral Resources Investigation and Evaluation Center, Xian 710054, China*

Correspondence should be addressed to Shoushi Gao; gaoshoushi8@163.com

Received 6 July 2023; Revised 9 October 2023; Accepted 13 October 2023; Published 3 November 2023

Academic Editor: Ying Qin

In order to address the issue of slow excavation speed caused by various factors affecting the stability of the roof in the excavation face and the unreasonable distance of the unsupported roof, a mechanical model of the roof in the excavation face area is established. This model is based on the superposition method in the material mechanics. The immediate roof deflection curve equation and the maximum unsupported roof distance discriminant formula of the heading head are derived. The allowable deflection is used as the discriminant method of the maximum unsupported roof distance. The calculation method of the key parameters in the formula is obtained and compared with the existing maximum unsupported roof distance calculation formula. Using the single-variable sensitivity analysis method and the bivariate interaction analysis method, we determine the key factors affecting the deformation of the roof in the excavation face and their interaction relationships. The results indicate that among the 10 factors affecting the deformation of the roof in the temporary support area of the excavation face, there are 3 key factors. Under unchanged geological and mechanical conditions, the deformation of the roof primarily depends on the length of the temporary support area and the temporary support load. To provide a practical example, we calculate the maximum unsupported roof distance of 30304 tailgate in the Yanghuopan Coal Mine to be 3.4 m. Numerical simulation and field monitoring results confirm that the deformation of the roof in the excavation face is minimal, and the stability of the rock is good.

1. Introduction

In recent years, the technology for excavating roadways has advanced rapidly, and fast excavation is a crucial factor for efficient coal mining [1]. The speed of roadway development not only depends on the modernization level of the excavating equipment but also is closely connected with each production process. Comprehensive mechanized tunneling is currently the commonly adopted method for fast coal roadways, generally using the operating line combining a cantilever excavator and monomer jumbolter. The time consumed by the advance and retreat of the cantilever excavator and the handling of the monomer jumbolter affects the tunneling speed.

Therefore, the size of the cycle advance is a bottleneck that restricts the improvement of the speed of roadway excavation. Under the premise of ensuring safety, increasing the cycle advance, that is, increasing the unsupported roof distance, reducing the number of times the cantilever excavator advances, retreats, and transports the monomer jumbolter, thereby reducing the time occupied by this link, is an important way to achieve rapid excavation in coal lanes. Moreover, a larger unsupported roof distance can increase the working space, realize parallel operations of anchor bolts and anchor xcables, and significantly improve the speed of roadway excavation.

Many scholars from China and other countries have conducted extensive research on the characteristics of tunnel heading roof deformation, the determination of reasonable unsupported roof distances, and control techniques. This research has been conducted through theoretical and numerical simulation studies, achieving fruitful results. Chen et al. [2], Bai et al. [3], Zhang [4], and Ding et al. [5] have constructed mechanical models of thin plates and rock beams in

the unsupported roof zone with different fixed and simply supported forms. Various methods, such as the energy method [6], difference method, elasticity theory [7], and strength reduction [8, 9], have been used to study the stability, deformation characteristics, failure modes, and stress distribution of the rock beam model. This has led to the derivation of the formula for calculating the limit unsupported roof distance [10–12]. The research also analyzed the influence of factors such as support components [13] and the speed of roadway excavation [14] on the surrounding rock of the unsupported roof zone. However, it should also be noted that the structural characteristics of the roof itself, such as lithology and degree of fragmentation, can also affect this calculation [3, 15–17].

Chang et al. [18], Meng et al. [19], and Xie et al. [20–23] have focused on the phenomenon of large-scale collapse of the surrounding rock in the unsupported roof area of the excavation face. They have conducted research on the stress evolution characteristics and deformation failure laws of the surrounding rock in the unsupported roof area of the excavation face using simulation software such as ABAQUS and FLAC^{3D}. The results show that by changing the cross-sectional shape and layout of the tunnel and using support measures such as "bolt + shoulder anchor cable to resist the deformation of the surrounding rock, the stress distribution form of the roof has been optimized, and the stability of the surrounding rock in the tunnel roof area has been improved [24–28].

However, the stability of the surrounding rock in the unsupported roof zone of the excavation face is influenced not only by the unsupported distance but also by multiple factors, such as the overburden load of the immediate roof above, the support load of the temporary support area, the support load of the unstable area of permanent support, the peak abutment pressure of the fixed end of the immediate roof, the density of the immediate roof, the thickness of the immediate roof, the length of the temporary support area, the length of the unstable area of permanent support, the distance from the peak abutment pressure of the model to the coal wall, and the elastic modulus of the immediate roof [29–31]. While existing studies often consider the impact of individual factors, they seldom take into account their combined effects. Therefore, the current state of theoretical research is insufficient to meet the demands of rapid excavation, as it does not adequately consider the complex interplay of these factors [32, 33].

In light of this contradiction, this paper establishes a mechanical model for the roof in the excavation face. We combine elastic theory and numerical simulation to study the deformation characteristics of the roof in the temporary support area of the excavation face. Additionally, we propose a calculation method for the maximum unsupported roof distance. We investigate the influence of parameters such as roof pressure, elastic modulus, thickness, density, and support strength on roof stability. Key influencing factors are identified through sensitivity analysis of these parameters. The accuracy and rationality of the calculation formula for the maximum unsupported roof distance proposed in this paper are verified by comparing with existing research results. The method proposed in this paper is applied to the 30304 tailgate of Yanghuo Pan Coal Mine. The results provide valuable insights into the stability and control mechanism of the surrounding rock during the rapid excavation process.

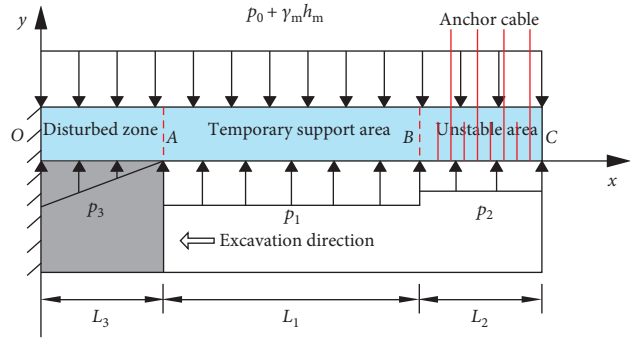

FIGURE 1: The mechanical model of the roof in the excavation area.

2. Analysis of Deformation Patterns in Temporary Support Zones during Roadway Excavation

2.1. Mechanical Model Design for Excavation Face. According to the stress form and support status of the roof and ribs during the roadway excavation process, the roadway can be divided into three zones in space: the disturbance zone of the tunnel excavation face, the temporary support zone, and the unstable zone of permanent support. The surrounding rock of the roadway gradually undergoes progressive damage from the shallow to the deep zones, and the roof of the temporary support zone is mainly affected by the damage of the shallow rock mass. However, due to the effect of temporary support, roof collapse and excessive subsidence are mitigated. Therefore, the immediate roof of the three zones near the heading face can be treated as a continuous structure, which is in the stage of elastic deformation and does not account for discontinuous plastic failure. The immediate roof of the middle section in the longitudinal direction of the excavation face zone is selected as the research object, and it is simplified as a fixed-hinged support at the left end and a fixed beam structure at the right end. The mechanical model is established, as depicted in Figure 1.

In the given context, the variables mentioned are related to the load and support conditions in a roadway excavation. The variables are defined as follows: p_0 is the load of the main roof acting on the immediate roof, $\gamma_m h_m$ is the self-weight load of the immediate roof, p_1 is the temporary support load of the heading face, p_2 is the support load of the unstable area of the permanent support, and p_3 is the support load of the coal wall to the immediate roof. L_1 is the length of the temporary support zone, L_2 is the length of the unstable zone of permanent support, and L_3 is the length of the disturbance zone of the excavation face.

2.2. Analysis of Deformation Law of Heading Face Roof. According to the principle of superposition, the deflection caused by multiple loads acting on a structure is equal to the

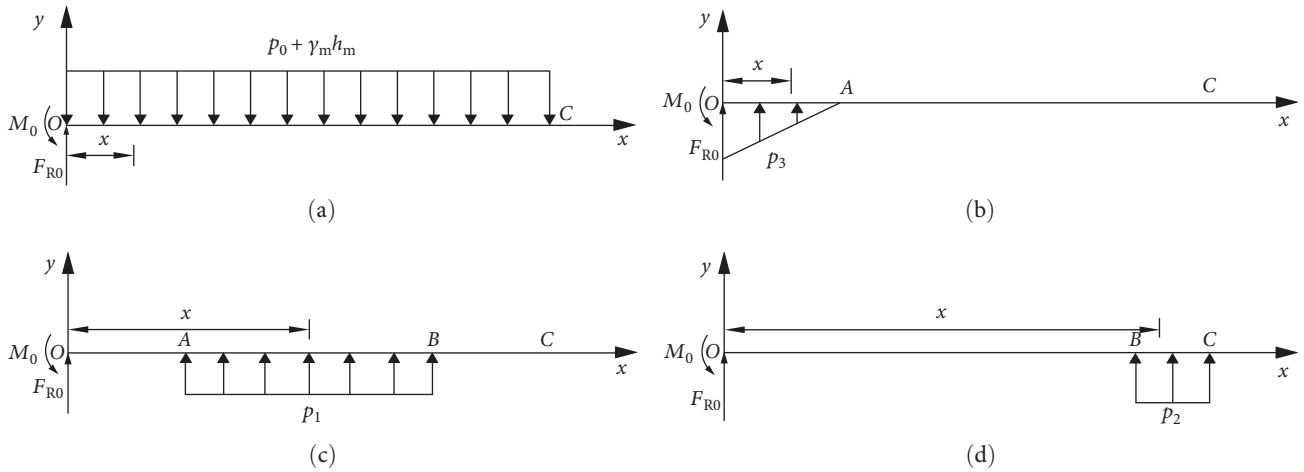

Figure 2: Calculation steps of superposition method: (a) first part; (b) second part; (c) third part; (d) fourth part.

sum of the deflections caused by each load acting individually on the structure. Therefore, to determine the deflection of the roof of the heading face, it is necessary to calculate the bending moment at point O when p_0, $\gamma_m h_m$, p_1, p_2, and p_3 act individually. Next, utilize Equation (1) for the deflection curve $w_i(x)$ and the angle of rotation $\theta_i(x)$ to calculate the deflections caused by each of the five types of loads separately. Finally, sum these deflections to obtain the total deformation of the model.

$$\begin{cases} \theta(x) = \int \dfrac{M(x)}{EI} dx + C \\ w(x) = \iint \dfrac{M(x)}{EI} dx + Cx + D. \end{cases} \tag{1}$$

In the above equation, E is the elastic modulus of the immediate roof, Pa; I is the moment of inertia of the cross-section of the unit width immediate roof rock beam, m^4, where $I = h_m^3/12$; h_m is the thickness of immediate roof, m.

2.2.1. Effect of p_0 and $\gamma_m h_m$. The force analysis of the model under the action of the uniformly distributed load p_0 and the self-weight $\gamma_m h_m$ of the rock layer is shown in Figure 2(a). Through deduction, the bending moment equation is obtained as follows:

$$M_{P_0+\gamma_m h_m}(x) = -0.5(p_0 + \gamma_m h_m)(L_0 - x)^2, x \in [0, L_0]. \tag{2}$$

In the above equation, L_0 is the total length of the model rock beam, m, where $L_0 = L_1 + L_2 + L_3$; p_0 is the load of the main roof acting on the immediate roof, Pa; γ_m is the bulk density of immediate roof, N/m^3; h_m is the thickness of immediate roof, m; x is the distance from any point on the immediate roof to point O (the rotation point of the model rock beam), m.

2.2.2. Effect of p_3. The load-bearing capacity of the solid coal wall, when subjected to the individual action of load p_3, can be analyzed as shown in Figure 2(b). Through deduction, the bending moment equation for the OA section can be obtained.

$$M_{P_3}(x) = \frac{p_3'(L_3 - x)^3}{6L_3}, x \in [0, L_3]. \tag{3}$$

In the above equation, L_3 is the distance between the peak stress of the fixed end of the model rock beam and the coal wall, m; p_3' is the peak load of the fixed end of the model rock beam, Pa.

2.2.3. Effect of p_1. When the temporary support load p_1 acts alone, the stress analysis is shown in Figure 2(c). The bending moment equation for the OB section can be obtained as follows:

$$M_{p_1}(x) = \begin{cases} p_1 L_1 (L_3 + 0.5L_1 - x), \ x \in [0, L_3] \\ 0.5p_1 (L_3 + L_1 - x), \ x \in [L_3, L_3 + L_1] \end{cases}. \tag{4}$$

In the above equation, p_1 is the temporary support load in the roof, Pa; L_1 is the length of the temporary support area, m; L_3 is the length of the disturbance zone of the excavation face, m.

2.2.4. Effect of p_2. When the load p_2 in the unstable zone of the permanent support acts alone, the stress analysis is shown in Figure 2(d). The bending moment equation in the OC section can be obtained as follows:

$$M_{p_2}(x) = \begin{cases} p_2 L_2 (L_1 + L_3 + 0.5L_2 - x), \ x \in [0, L_1 + L_3] \\ 0.5p_2 (L_0 - x), \ x \in [L_1 + L_3, L_0] \end{cases}. \tag{5}$$

In the above equation, p_2 is the support load in the unstable area of permanent support, Pa; L_2 is the length of the unstable zone of permanent support, m.

Therefore, the bending moment equation of the immediate roof beam is as follows:

$$M(x)=\begin{cases}-\dfrac{(p_0+\gamma_m h_m)(L_0-x)^2}{2}+\dfrac{p_3'(L_3-x)^3}{6L_3}+p_1L_1(L_3+0.5L_1-x)+p_2L_2(L_1+L_3+0.5L_2-x),[0,L_3]\\ -\dfrac{(p_0+\gamma_m h_m)(L_0-x)^2}{2}+\dfrac{p_1(L_1+L_3-x)}{2}+p_2L_2(L_1+L_3+0.5L_2-x),[L_3,L_1+L_3]\\ -\dfrac{(p_0+\gamma_m h_m)(L_0-x)^2}{2}+\dfrac{p_2(L_0-x)}{2},[L_1+L_3,L_0].\end{cases}\tag{6}$$

According to Equations (1) and (6), the deflection curve equation of the immediate roof in the temporary support area of the heading face can be obtained as follows:

$$w(x)=-\frac{(p_0+\gamma_m h_m)(L_0-x)^4}{24EI}+\frac{p_1(L_1+L_3-x)^3}{12EI}+\frac{p_2L_2(L_1+L_3+0.5L_2-x)^3}{6EI}+Cx+D,x\in[L_3,L_1+L_3].\tag{7}$$

Considering the boundary conditions, $\theta(0)=0$ and $w(0)=0$, by combining Equations (1) and (8), the constant C and D can be solved to obtain the analytical expression.

$$\begin{cases}C=-\dfrac{(p_0+\gamma_m h_m){L_0}^3}{6EI}+\dfrac{p_3'{L_3}^4}{24L_3EI}+\dfrac{p_1L_1(L_3+0.5L_1)^2}{2EI}+\dfrac{p_2L_2(L_1+L_3+0.5L_2)^2}{2EI}\\ D=\dfrac{(p_0+\gamma_m h_m){L_0}^4}{24EI}-\dfrac{p_3'{L_3}^5}{120L_3EI}-\dfrac{p_1L_1(L_3+0.5L_1)^3}{6EI}-\dfrac{p_2L_2(L_1+L_3+0.5L_2)^3}{6EI}.\end{cases}\tag{8}$$

3. Determination of the Distance between the Unsupported Roof Zone of the Excavation Face

3.1. Derivation of Unsupported Roof Distance of Excavation Face. According to Equation (7), it can be inferred.

$$w'(x)<0,x\in[L_3,L_1+L_3].\tag{9}$$

The equation for the deflection curve $w'(x)$ indicates that the minimum value occurs at $x=L_1+L_3$. This implies that the maximum subsidence position of the temporary support area of the excavation face occurs at $x=L_1+L_3$, with a corresponding maximum subsidence value of the following:

$$w_{\max}=-\frac{(p_0+\gamma_m h_m){L_2}^4}{24EI}+\frac{p_2L_2(0.5L_2)^3}{6EI}+C(L_1+L_3)+D.\tag{10}$$

When $p_1=0$, which means that the roof of the excavation face is in an unsupported state, the allowable deflection $[w]$ is used as the maximum limit for the deformation of the roof, as shown in Equation (11).

$$w_{\max}<[w]\tag{11}$$

$$w_{\max}=-\frac{(p_0+\gamma_m h_m){L_2}^4}{24EI}+\frac{p_2L_2(0.5L_2)^3}{6EI}+C_1(L_1+L_3)+D_1<[w],\tag{12}$$

where C_1 and D_1 are as follows:

$$\begin{cases}C_1=-\dfrac{(p_0+\gamma_m h_m){L_0}^3}{6EI}+\dfrac{p_3'{L_3}^4}{24L_3EI}+\dfrac{p_2L_2(L_1+L_3+0.5L_2)^2}{2EI}\\ D_1=\dfrac{(p_0+\gamma_m h_m){L_0}^4}{24EI}-\dfrac{p_3'{L_3}^5}{120L_3EI}-\dfrac{p_2L_2(L_1+L_3+0.5L_2)^3}{6EI}.\end{cases}\tag{13}$$

According to Equations (12) and (13), the numerical solution of the maximum distance L_1 of the excavation face roof in an unsupported state can be obtained.

3.2. Parameter Calculation. According to Equations (12) and (13), the maximum distance of the unsupported roof of the excavation face is related to the following eight parameters:

(1) immediate roof overburden load p_0,
(2) support load p_2 of the permanent support unstable zone,
(3) peak load p_3' of the coal wall supporting the fixed end to the immediate roof,
(4) the bulk density γ_m of the immediate roof,
(5) the thickness h_m of the immediate roof,
(6) the length L_2 of the unstable area of the permanent support,
(7) the distance L_3 between the peak stress of the fixed end of the model rock beam and the coal wall,
(8) the elastic modulus E of the immediate roof. Among them, the parameters of p_3', γ_m, h_m, L_2, and E can be easily obtained through practical measurements. The parameters of p_0, p_2, and L_3 can be obtained through theoretical calculations, and their calculation methods are as follows.

3.2.1. The Distance L_3 from the Stress Peak at the Fixed Support End of the Model to the Coal Wall. In front of the coal wall, a small plastic element with a span of dx is taken along the x-axis excavation direction, as shown in Figure 3. The shear force τ and the vertical stress σ_y of the plastic microelement model along the x-axis direction satisfy the Mohr–Coulomb strength criterion.

$$\tau = \sigma_y \tan\varphi_0 + c_0. \tag{14}$$

In the above equation, τ is the shear force of the interface between the coal seam and the roof along the x-axis direction, Pa; σ_y is the maximum principal stress, Pa; φ_0 is the internal friction angle between the coal seam and the roof interface, °; c_0 is the cohesion of the interface between the coal seam and roof, Pa.

The following equilibrium equations can be established at any position in the limit equilibrium zone:

$$M\sigma_x + 2\left(\sigma_y \tan\varphi_0 + c_0\right)dx - M(\sigma_x + d\sigma_x) = 0. \tag{15}$$

In the equation, M is the roadway height, m; σ_x minimum principal stress, Pa.

The selected microelement is in the limit equilibrium zone, so the maximum principal stress and the minimum principal stress satisfy the Mohr–Coulomb strength criterion.

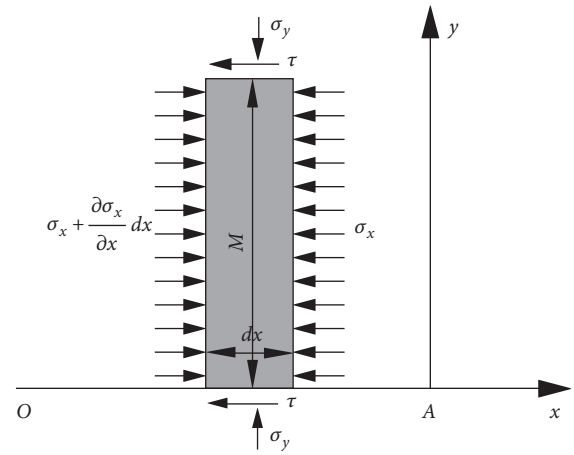

FIGURE 3: Plastic infinitesimal model of limit equilibrium zone in front of coal wall.

$$\sigma_y = 2c\sqrt{\frac{1+\sin\varphi}{1-\sin\varphi}} + \frac{1+\sin\varphi}{1-\sin\varphi}\sigma_x. \tag{16}$$

In the above equation, c is the cohesion of coal, Pa; φ is the internal friction angle of coal.

Let: $R_c = 2c\sqrt{\frac{1+\sin\varphi}{1-\sin\varphi}}$, $R_\varphi = \frac{1+\sin\varphi}{1-\sin\varphi}$.

Where σ_y is as follows:

$$\sigma_y = R_c + R_\varphi \sigma_x. \tag{17}$$

By differentiating the Equation (17), we get the following:

$$d\sigma_y = R_\varphi d\sigma_x. \tag{18}$$

By substituting Equation (18) into the equilibrium Equation (15), the expression for the vertical and horizontal stress components in the plastic zone can be obtained [5].

$$\sigma_y = \eta e^{\frac{2R_\varphi \tan\varphi_0}{M}x} - \frac{c_0}{\tan\varphi_0}. \tag{19}$$

$$\sigma_x = \frac{\eta}{R_\varphi} e^{\frac{2R_\varphi \tan\varphi_0}{M}x} - \frac{2c\cos\varphi}{1+\sin\varphi} - \frac{c_0}{R_\varphi \tan\varphi_0}. \tag{20}$$

In the above equation, η is the integration constant. Since at point A ($x = 0$), the horizontal stress boundary condition $\sigma_x = 0$, the expression for η can be calculated as follows:

$$\eta = \frac{2c\cos\varphi}{1-\sin\varphi} + \frac{c_0}{\tan\varphi_0}. \tag{21}$$

By substituting Equation (21) into Equation (20), we can obtain the expression for the vertical stress along the y-axis at any point within the OA section in front of the coal wall.

Table 1: Calculation parameters of the maximum unsupported roof distance of the plate model.

Roadway width a (m)	Thickness of separated rock mass h (m)	Tensile strength σ_t (MPa)	Uniformly distributed load q (MPa)
4.6	0.87	3.67	0.191

Table 2: Theoretical calculation parameters of maximum unsupported roof distance.

Overburden load p_0 (MPa)	Support load p_2 (MPa)	Peak load p_3' (MPa)	Bulk density γ_m (kN/m^3)	Thickness h_m (m)	Length of unstable zone L_2 (m)	Length of limit equilibrium zone L_3 (m)	Elastic modulus E (GPa)
0.191	0.19	35.1	25.8	7.4	2.579	0.579	18.5

$$\sigma_y = \left(\frac{2c\cos\varphi}{1-\sin\varphi} + \frac{c_0}{\tan\varphi_0}\right)e^{\frac{2R_\varphi \tan\varphi_0}{M}x} - \frac{c_0}{\tan\varphi_0}. \quad (22)$$

At point O ($x = L_3$), the stress in the y-direction (σ_y) is equal to $K\gamma H$, which allows us to solve for L_3.

$$L_3 = \frac{M}{2R_\varphi \tan\varphi_0}\ln\frac{(1-\sin\varphi)(\tan\varphi_0 K\gamma H + c_0)}{2c\cos\varphi\tan\varphi_0 + c_0(1-\sin\varphi)}. \quad (23)$$

3.2.2. Immediate Roof Overburden Load p_0. The force exerted on the excavation face by the immediate roof is the sum of the overburden loads. In general, for the convenience of calculation, the strata load is assumed to be uniformly distributed. According to the principle of composite beams, we can determine the magnitude of the overburden load p_0 on the excavation face [10].

$$(q_n)_1 = \frac{E_1 {h_1}^3(\gamma_1 h_1 + \gamma_2 h_2 + \cdots + \gamma_n h_n)}{E_1 {h_1}^3 + E_1 {h_1}^3 + \cdots + E_n {h_n}^3}. \quad (24)$$

In the above equation, $(q_n)_1$ is the load acting on the first layer by the nth layer, Pa; E_n is the elastic modulus of the nth layer, Pa; h_n is the thickness of the nth layer, m; γ_n is the volume force of the nth layer, N m$_\gamma^{-3}$.

When the calculated result $(q_n)_1 > (q_{n+1})_1$, it indicates that the $n+1$ layer of rock strata, due to its characteristics of high strength and thickness, does not exert any load on the first layer of rock strata. In this case, the q value represents the load p_0 exerted by the combined action of the main roof of the n layers in the unsupported roof area.

3.2.3. Supporting Load p_2 in Unstable Area of Permanent Support. The relative movement of the roof surrounding the roadway exerts tension forces on the bolts and anchor cables. The bolts and anchor cables suspend the immediate roof from the firm and stable main roof. Therefore, the support load p_2 provided by the bolts and anchor cables in the unstable area behind the excavation face of the roadway is calculated using the suspension theory.

$$p_2 = \frac{n}{S_1}q_n + \frac{m}{S_2}q_m. \quad (25)$$

In the above equation, p_2 is the total load on the unstable area of permanent support, Pa; n is the number of bolts in the support area; S_1 is the suspended area of the bolts in the support area, m^2; q_n is the anchoring force of the bolts, N; m is the number of anchor cables in the support area; S_2 is the suspended area of the anchor cables in the support area, m^2; and q_m is the anchoring force of the anchor cables, N.

3.3. Comparative Analysis of Calculating Models for Maximum Unsupported Roof Distance

3.3.1. Calculation of the Maximum Unsupported Roof Distance of the "Plate" Model. To validate the accuracy of the calculation method for the maximum unsupported roof distance proposed in this paper, a comparative analysis is conducted with the findings of previous research. Li Jie [23] derived the calculation Equation (26) for the maximum unsupported roof distance using a "plate" model and concluded that the critical value (σ_{max}) for roof failure in the unsupported roof area of the excavation face is equal to the ultimate tensile strength (σ_t). Using the calculation parameters listed in Table 1, the maximum unsupported roof distance for tailgate 110 in the Dangjiahe Coal Mine was calculated to be 4.8 m.

$$b = \sqrt[4]{\frac{a^2h^2\pi^2\sigma_t(3a^2+2b^2)}{12qa^2 - 3h^2\pi^2\sigma_t}}, \quad (26)$$

where a is the roadway width, m; b is the maximum unsupported roof distance, m; σ_t is the tensile strength of the immediate roof, Pa; q is the uniform load on the immediate roof, Pa; h is the thickness of the shallow separated rock mass in the unsupported roof area, m.

3.3.2. Calculation of the Maximum Unsupported Roof Distance of the "Beam" Model. Equation (12), for calculating the maximum unsupported roof distance, is derived in this paper using the "beam" model. The calculation parameters for the tailgate 110 of the Dangjiahe Coal Mine are listed in Table 2. The maximum roof subsidence curve of the tailgate 110 at different unsupported roof distances is plotted in Figure 4. The allowable deflection [w] is used as the maximum limit for the deformation of the unsupported roof, which means that the maximum deflection w_{max} of the unsupported roof failure in the excavation face is equal to the allowable deflection [w]. Therefore, the maximum unsupported roof distance of the tailgate 110 is calculated to be 4.08 m.

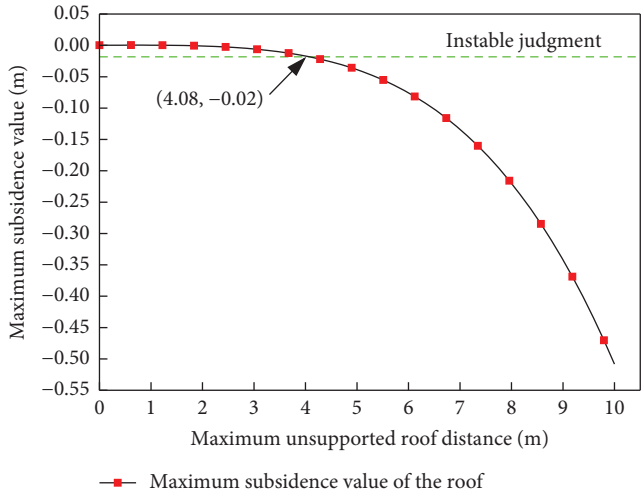

FIGURE 4: Maximum subsidence curve of the roof.

According to the analysis above, it can be concluded that Li Jie's [18] calculation method for determining the maximum unsupported roof distance, the calculation assumed that the permanent support zone behind the unsupported roof area remains stable. However, the calculation does not consider the impact of advancing abutment pressure within the coal wall on the unsupported roof area. As a result, the calculation tends to overestimate the maximum unsupported roof distance when compared to the actual conditions.

Therefore, when the influence of the coal wall in front of the advancing unsupported roof area and the support area behind it on the stability of the surrounding rock in the unsupported roof area is relatively small, Li Jie's calculation method demonstrates greater adaptability and the calculation results exhibit higher accuracy. This method is particularly applicable to advancing working faces with a hard roof and enables rapid attainment of the design standard for support quality. However, the calculation method derived in this paper demonstrates greater adaptability for heading faces with poor roof conditions and complex geological conditions.

4. The Analysis of Influencing Factors on the Deformation of Temporary Support Area in Heading Face of Roadway Excavation

4.1. Single Factor Sensitivity Analysis and Determination of Key Influencing Factors. Univariate sensitivity analysis is the most commonly used method for parameter sensitivity analysis. It is a local analysis approach, also known as the single-factor analysis method. The main steps involve holding the baseline values of all parameters except the one being analyzed constant and only changing the value of one parameter at a time. By comparing the magnitude of change in the output, different parameter sensitivities can be determined.

4.1.1. Scheme Design. According to Equations (7) and (8), the roof deformation of the temporary support area in the heading face of the roadway is related to a total of 10 influencing factors. Factor 1: the overburden load p_0 of the immediate roof. Factor 2: the support load p_1 of the temporary support area. Factor 3: the support load p_2 of the unstable area of permanent support. Factor 4: the peak load p_3' of the coal wall to the immediate roof. Factor 5: the bulk density γ_m of the immediate roof. Factor 6: the thickness h_m of the immediate roof. Factor 7: the length L_1 of the temporary support area. Factor 8: the length L_2 of the unstable area of permanent support. Factor 9: the distance L_3 between the peak stress of the immediate roof and the coal wall. Factor 10: the elastic modulus E of the immediate roof. By the origin function fitting manager, Equation (7) is used to analyze the sensitivity of each variable on the deformation of the temporary support area in the heading face of the roadway, thereby determine the key influencing variables. Table 3 presents the calculation parameters used in the case study.

4.1.2. Determination of Key Influencing Factors. The analysis was conducted by running the model for each case presented in Table 3. The variations in roof displacement are shown in Figure 5. It can be observed that among the single-parameter variations, the thickness of the immediate roof (h_m), the distance between the peak stress of the immediate roof and the coal wall (L_3), and the length of the temporary support zone (L_1) have the greatest influence on the roof displacement in the unsupported roof area. The maximum displacements for these three factors are 0.884, 0.223, and 0.221 m, respectively. These three variables are key factors affecting the subsidence of the roof in the excavation face of the roadway. Therefore, they are considered key factors affecting the subsidence of the roof in the excavation face of the roadway.

The other parameters considered are the overburden load on the immediate roof (p_0), the length of the unstable zone of permanent support (L_2), the elastic modulus of the immediate roof (E), and the support load of the temporary support zone (p_1). The maximum subsidence values for these parameters are 0.168, 0.136, 0.073, and 0.063 m. These four factors are secondary factors that affect the roof subsidence in the excavation face of the roadway.

The support load of the unstable zone of permanent support (p_2), the peak load of the coal wall on the immediate roof (p_3'), and the bulk density of the immediate roof (γ_m) have the least influence on the roof deformation.

4.2. Interaction Analysis of Support Load p_1 and Length L_1 in Temporary Support Area. If the actual working conditions are determined, the deformation of the temporary support area depends on the support length L_1 and the support load p_1.

4.2.1. Example Design. A two-factor interaction design was performed to evaluate the impact of support load (p_1) and the length (L_1) of the temporary support area. The support load (p_1) was varied from 0 to 10 MPa, while the length (L_1) of the support area was varied from 0 to 5 m. Other parameters used in the study included the immediate roof overburden load ($p_0 = 5$ MPa), support load ($p_2 = 0.5$ MPa) in the unstable area of permanent support, peak support load ($p_3' = 5$ MPa) at the fixed end of the coal wall for the direct roof, direct roof bulk density ($\gamma_m = 24$ kN/m^3), immediate

Table 3: Calculation parameters of example.

Example	Overburden load p_0 (MPa)	Support load p_1 (MPa)	Support load p_2 (MPa)	Peak load p_3' (MPa)	The bulk density γ_m (kN/m^3)	Thickness h_m (m)	The length L_1 (m)	The length L_2 (m)	The length L_3 (m)	Elastic modulus E (GPa)
Example 1	2–8	2	0.5	5	24	2	3	2	2	10
Example 2	5	2–8	0.5	5	24	2	3	2	2	10
Example 3	5	2	0.2–0.8	5	24	2	3	2	2	10
Example 4	5	2	0.5	2–8	24	2	3	2	2	10
Example 5	5	2	0.5	5	18–30	2	3	2	2	10
Example 6	5	2	0.5	5	24	1.0–3.5	3	2	2	10
Example 7	5	2	0.5	5	24	2	1.5–4.5	2	2	10
Example 8	5	2	0.5	5	24	2	3	0.5–3.5	2	10
Example 9	5	2	0.5	5	24	2	3	2	0.5–3.5	10
Example 10	5	2	0.5	5	24	2	3	2	2	7–13
Sensitivity	Sensitivity	Sensitivity	Insensitivity	Insensitivity	Insensitivity	Sensitivity	Sensitivity	Sensitivity	Sensitivity	Sensitivity

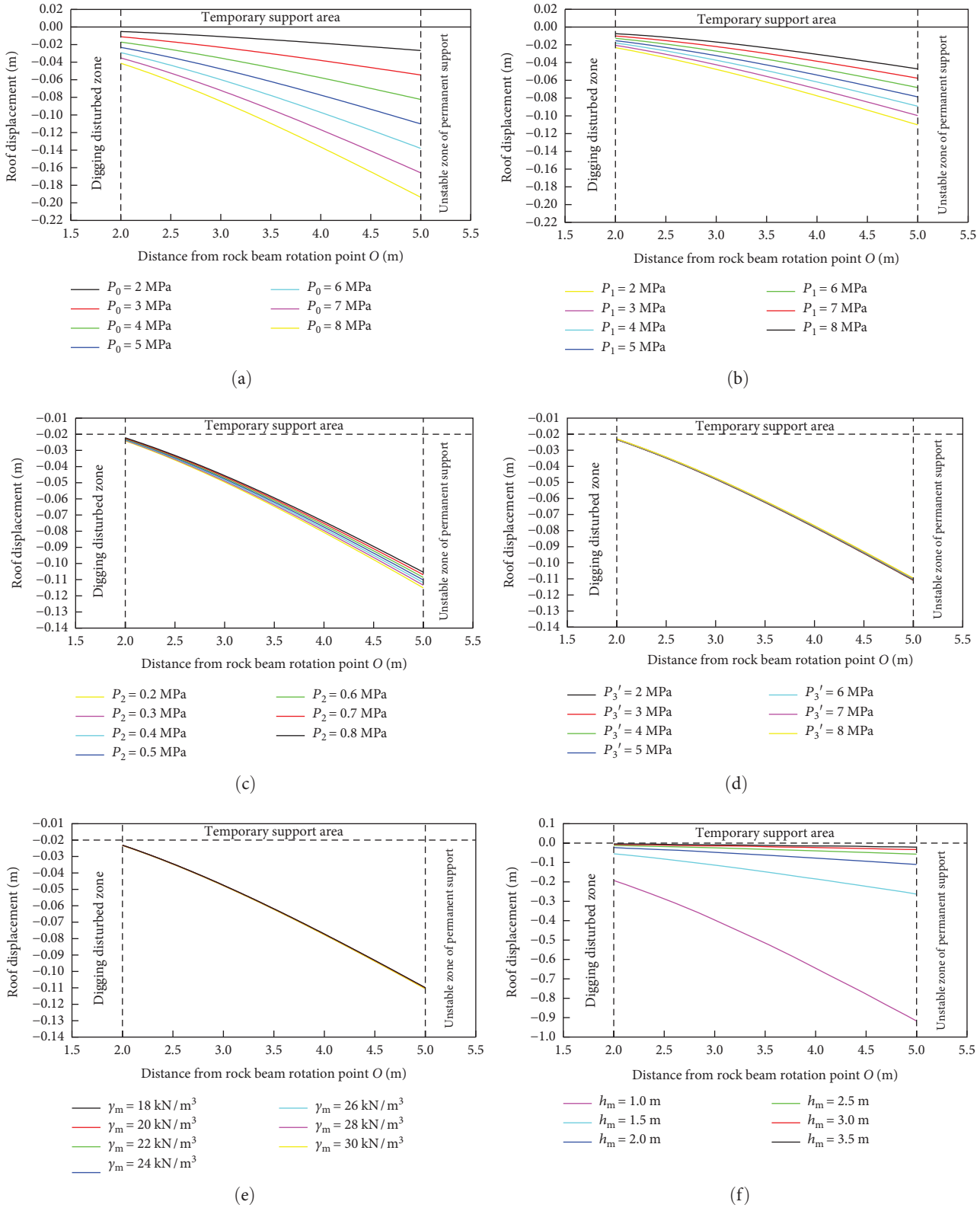

Figure 5: Continued.

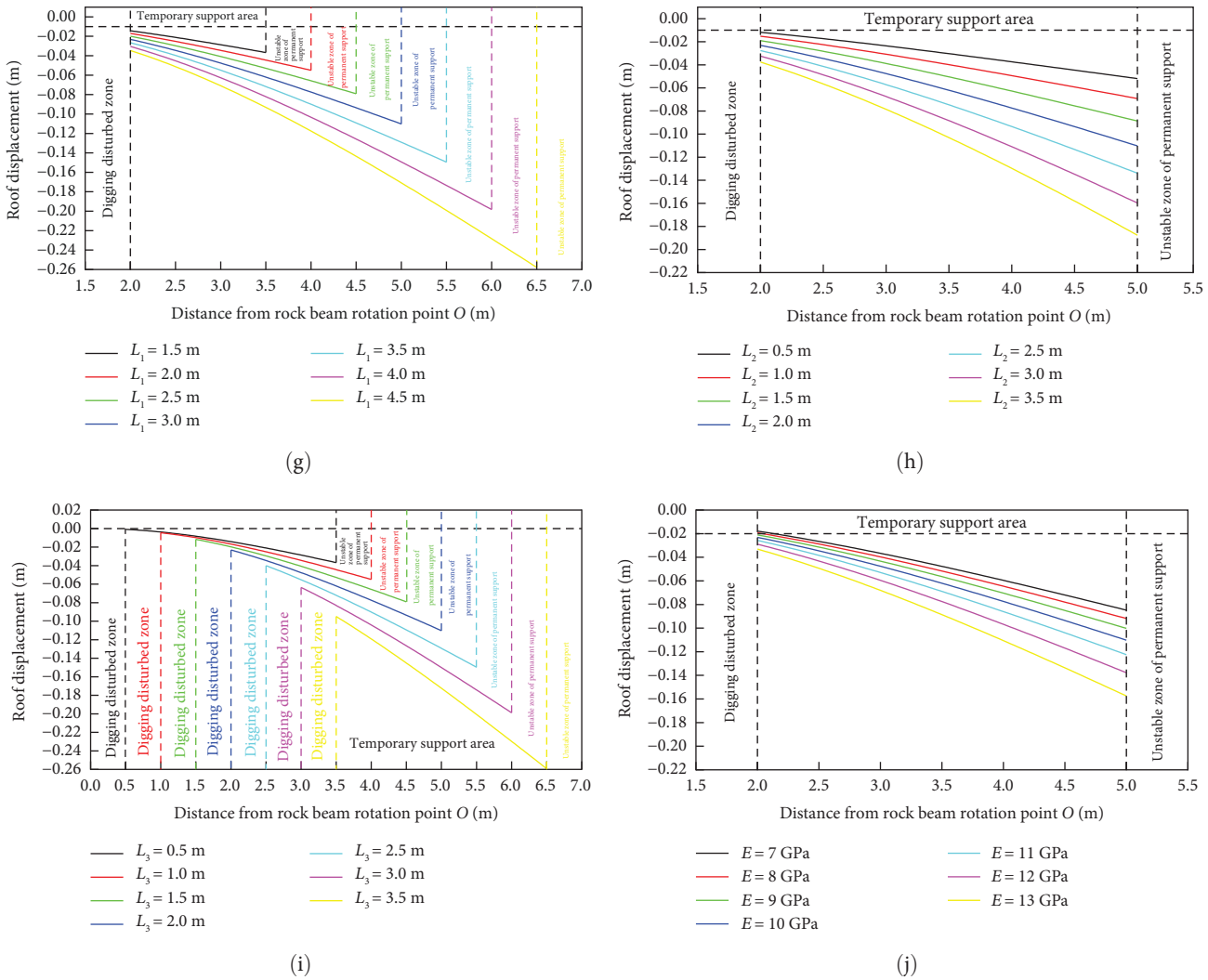

Figure 5: Univariate sensitivity analysis: (a) Example 1; (b) Example 2; (c) Example 3; (d) Example 4; (e) Example 5; (f) Example 6; (g) Example 7; (h) Example 8; (i) Example 9; (j) Example 10.

roof thickness ($h_m = 2$ m), length of unstable area of permanent support ($L_2 = 2$ m), distance between the peak stress of model rock beam and the coal wall ($L_3 = 2$ m), and elastic modulus ($E = 10$ GPa).

4.2.2. Analysis of Roof Subsidence under Interaction. According to Equations (7) and (8), the displacement of the temporary support zone roof at the maximum subsidence position ($x = L_1 + L_3$) can be plotted against the interaction between the support load p_1 and the length L_1 of the support zone, as shown in Figure 6. When the support load in the temporary support zone is constant, the subsidence of the roof increases with the increase in the length of the support zone. After the support zone length L_1 exceeds 4.0 m, the sinking rate of the roof significantly accelerates, and effective control of the sinking of the roof can be achieved by increasing the temporary support load. Therefore, the determination of a reasonable support load and support length for the temporary support zone is crucial for controlling the roof under unchanged working conditions.

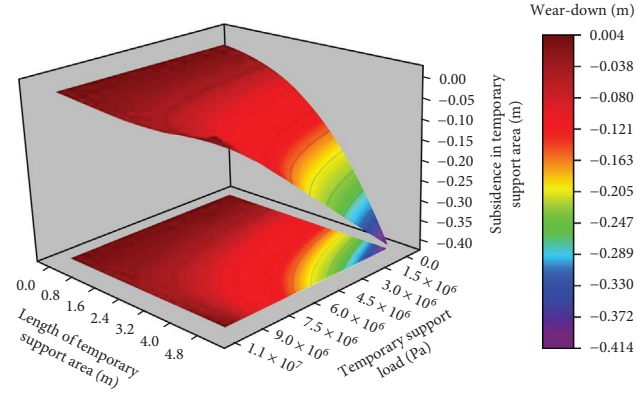

Figure 6: Roof subsidence surface.

5. Engineering Example

5.1. Project Profile. Yanghuopan Coal Mine is situated in the southwest of the Xinmin mining area in the Shenfu mining area of the Jurassic coalfield in northern Shanxi. The average

Number	Lithology	Thick (m)	Histogram
1	Loess	22.4	
2	Fine sandstone	12.1	
3	Siltstone	1.8	
4	Fine sandstone	13.53	
5	Medium sandstone	22.47	
6	Siltstone	9.54	
7	Fine sandstone	3.74	
8	Siltstone	9.42	
9	3-1 Coal	2.15	
10	Siltstone	4.63	
11	Fine sandstone	8.05	

Figure 7: Coal strata histogram.

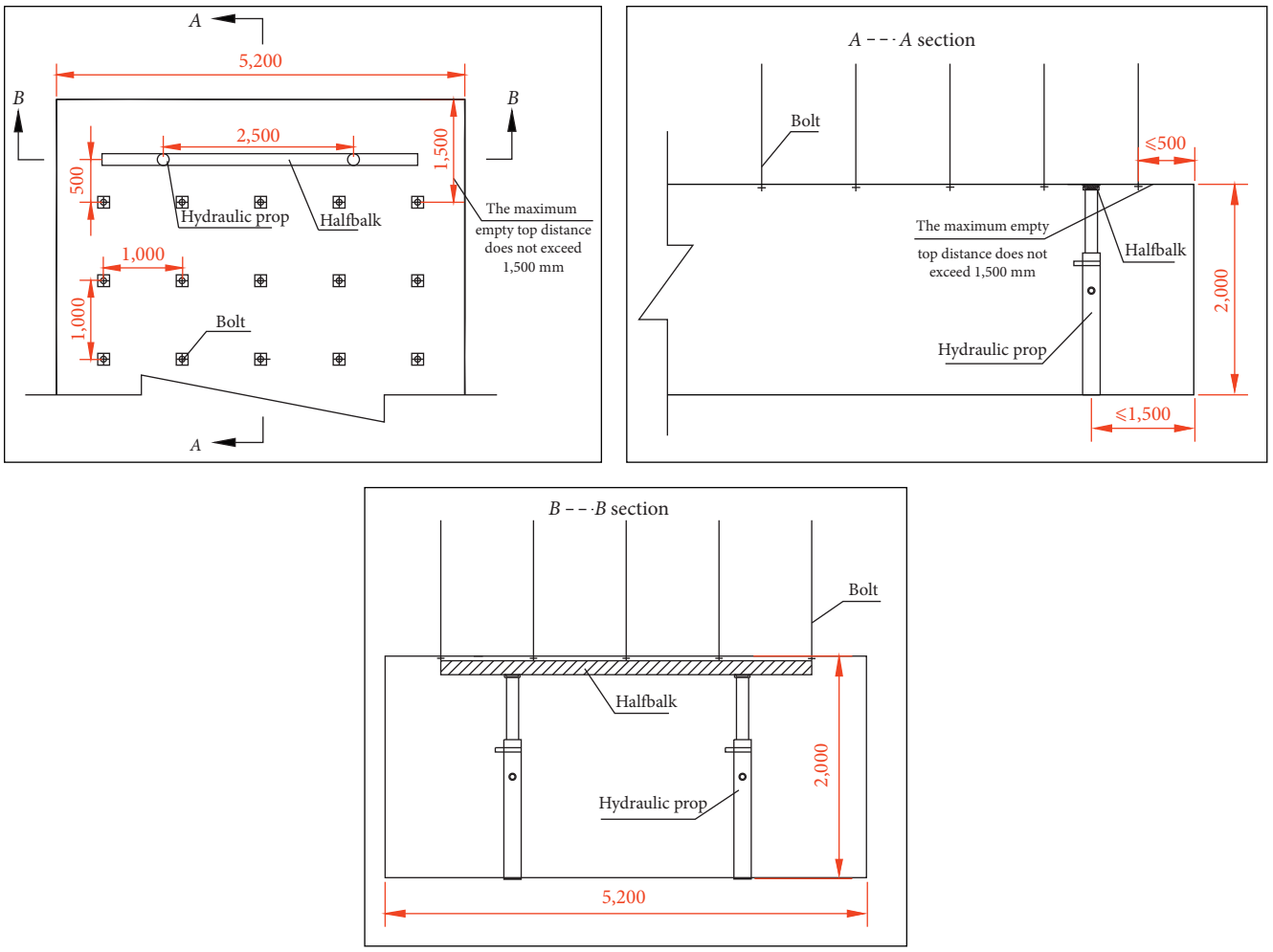

Figure 8: Temporary support diagram.

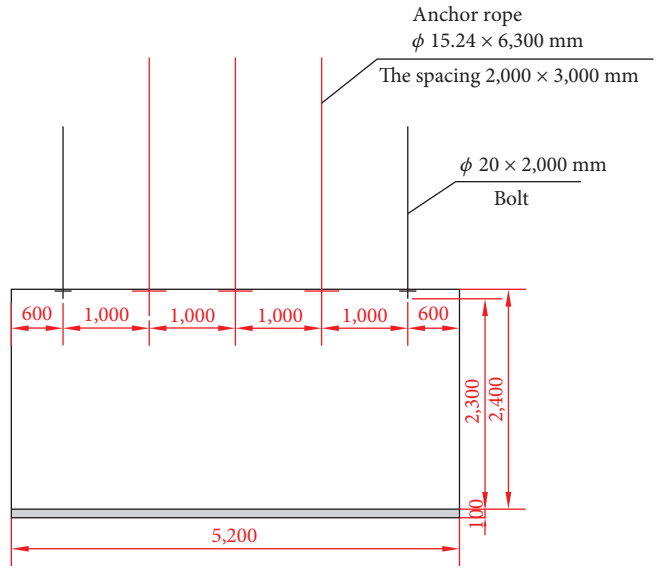

Figure 9: Roadway permanent support section diagram.

thickness of the coal seam in the 30304 panel is 2.15 m, with a dip angle of 1°. The 30304 tailgate runs along the floor of the 3^{-1} coal seam, with a roof elevation ranging from +1,126.3 to +1,210 m. The roadway has a rectangular section with a net width of 5.2 m and a net height of 2.3 m. Currently, the maximum unsupported roof distance is not more than 1.5 m, and the minimum unsupported roof distance is not more than 0.5 m, with each operation cycle being 1 m. This limits the distance of the excavator into the roadway at one time, leading to frequent alternation of excavation and support processes, which adversely affect the speed of roadway excavation.

The immediate roof of the 30304 tailgate is composed of 9.42 m of siltstone. The floor is also composed of siltstone with a thickness of 4.63 m and a saturated compressive strength of 10.1 MPa. The main roof is mainly composed of siltstone and fine-grained sandstone, with a uniaxial compressive strength of 24.1 MPa in a dry state. The columnar diagram of the coal and rock layer in the working face is shown in Figure 7.

5.2. Excavation Face Support Method

5.2.1. Temporary Support Method. For the temporary support during the excavation of the 30304 tailgate, it is recommended to use two single hydraulic props and one semicircular wood frame shed. The spacing between each hydraulic prop and the shed should be 2,500 mm. The semicircular wood frame shed should have a minimum diameter of 180 mm and a minimum length of 4.0 m. The supporting height for a single hydraulic prop should be between 2.2 and 2.5 m. It is important to regularly assess and tighten the temporary support as needed. The semicircular wood should be positioned in close to the roof. A schematic diagram of the temporary support is shown in Figure 8.

5.2.2. Permanent Support Method. The permanent support for the 30304 tailgate consists of a combination of bolts, steel mesh, and anchor cables. The two sides are not supported, and the concrete floor is constructed after the roadway has been built. Figure 9 provides a schematic diagram of the roadway section support, while the main support parameters are listed below:

(1) The roof bolts are arranged in rows, with each row consisting of 5 bolts. The spacing between the bolts is 1,000 × 1,000 mm. These bolts are made of Φ20 × 2,000 mm screw steel, specifically mmg 335 steel. The iron support plate, also made of mmg 335 steel, has dimensions of 150 × 150 × 10 mm. To secure the bolts, a CK23/60 resin cartridge is used for each bolt.

(2) The steel mesh is made of 6 mm diameter steel bars, with a mesh size of 100 × 100 mm. The mesh panel size is 1,200 × 4,700 mm. Each row uses one piece of steel mesh, with a minimum overlap size of 100 mm between adjacent rows.

(3) The arrangement of roof anchor cables in the roadway follows a "212" pattern along the centerline. The spacing between each anchor cable is 2,000 × 3,000 mm. The anchor cables have dimensions of Φ15.24 × 6,300 mm, while the iron support plates measure 300 × 300 × 10 mm. Each anchor cable requires the use of three CK35/40 resin cartridges.

5.3. Calculation of Maximum Unsupported Roof Distance. The paragraph provides an analysis of the maximum unsupported roof distance in the context of the Yanghuopan Coal Mine. It utilizes calculation Equation (12) and the calculation parameters listed in Table 4 to determine the maximum subsidence curve of the roof for the 30304 tailgate, as shown in Figure 10. The purpose of plotting this curve is to assess the stability of the roof and establish the maximum allowable deflection $[w]$. Through calculation, it has been determined that the maximum unsupported distance of the 30304 tailgate in the Yanghuopan Coal Mine is 3.4 m.

Table 4: Calculation parameters of the maximum unsupported roof distance of 30304 tailgate.

Overburden load p_0 (MPa)	Support load p_2 (MPa)	Peak load p_3' (MPa)	The bulk density γ_m (kN/m^3)	Thickness h_m (m)	The length L_2 (m)	The length L_3 (m)	Elastic modulus E (GPa)
1.193	0.0235	4.7	22.4	4.15	3.0	0.67	16.5

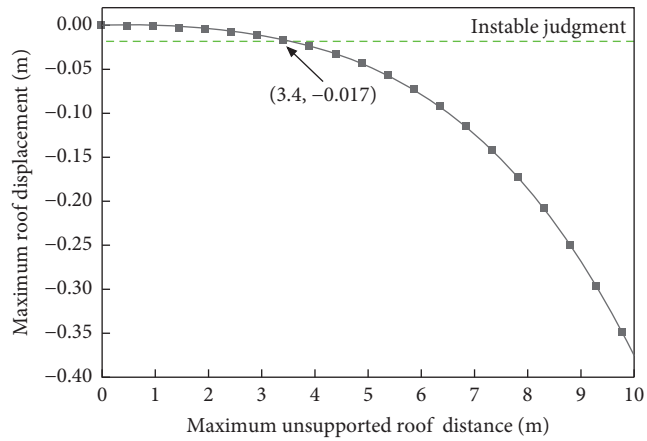

Figure 10: The maximum subsidence curve.

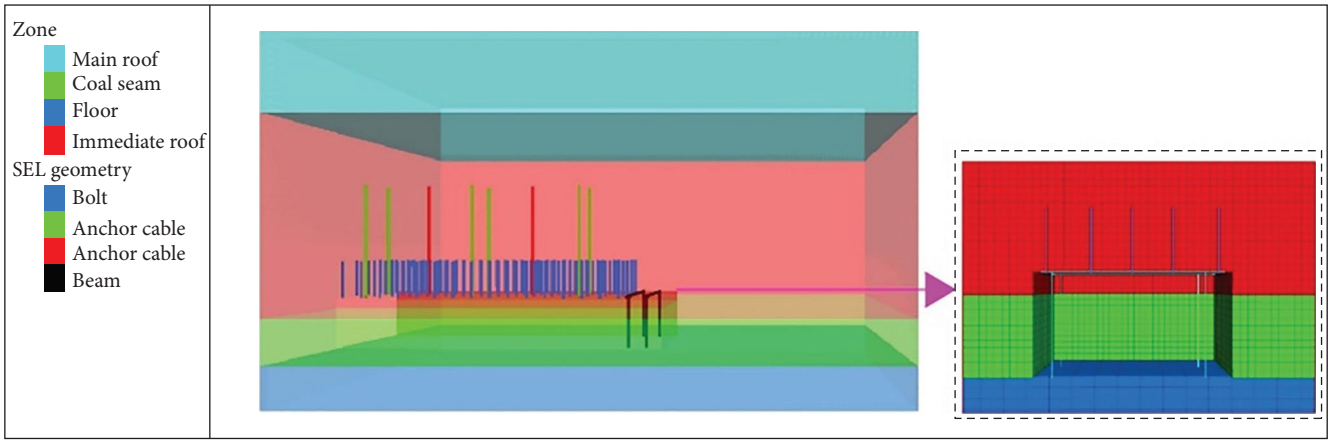

Figure 11: Calculation model.

5.4. Temporary Support Zone Numerical Simulation Analysis. This section presents an analysis of the rationality of the temporary support parameters in the roadway of the Yanghuopan Coal Mine using the FLAC^{3D} numerical simulation software. The geological conditions of the mine are taken into consideration. The calculation model, as depicted in Figure 11, includes a roof temporary support zone with a distance of 3.4 m. Temporary support is provided by four individual hydraulic props and two semicircular timbers. The support components in the temporary support area are simulated using beam structural elements. The specific support parameters can be found in Table 5.

Displacement constraints are applied to the lower part of the model, while the upper part and the surrounding areas are subjected to stress boundary conditions with a magnitude of 3.75 MPa. The initial horizontal stress is equivalent to the vertical stress. A stress gradient of 25,000 N/m is established to vary with depth. The entire model is influenced by a gravitational acceleration of 9.81 m/s^2. The Mohr–Coulomb model is selected as the constitutive model for simulating the behavior of the rock formation. The mechanical parameters of the coal-rock model are determined using geological data and laboratory rock physics experiments, as presented in Table 6. Upon reaching equilibrium, an analysis is conducted to examine the stress, displacement, and distribution of plastic zones in the surrounding rock of the tailgate.

Figure 12 illustrates the contour map depicting the distribution of vertical stress within the temporary support area. The figure reveals that the stress in the shallow surrounding rock of the temporary support area's roof exhibits minimal variation. Conversely, the stress range gradually extends to deeper rock layers in the two sides of the roadway and the

Table 5: Parameters of bolt and anchor cable.

Name	Diameter (mm)	Length (mm)	Spacing (mm × mm)	Quantity	Preload (kN)	Elastic modulus (Pa)	Cohesive force (Pa)	Stiffness of anchoring agent (Pa)
Bolt	20	2,000	1,000 × 1,000	5	80	2×10^{10}	1×10^{5}	2×10^{7}
Anchor cable	15.24	6,300	2,000 × 3,000	2/1/2	150	2.5×10^{10}	2×10^{5}	2×10^{7}

Table 6: Mechanical parameters of coal and rock.

Name	Density (kg/m^3)	Cohesion (MPa)	Tensile strength (MPa)	Angle of internal friction (°)	Shear modulus (GPa)
Floor	2,350	1.15	1.23	33	0.216
Immediate roof	2,100	0.76	0.90	32	0.314
Coal seam	1,350	0.20	0.59	30	0.312
Main roof	2,550	1.34	1.44	34	0.226

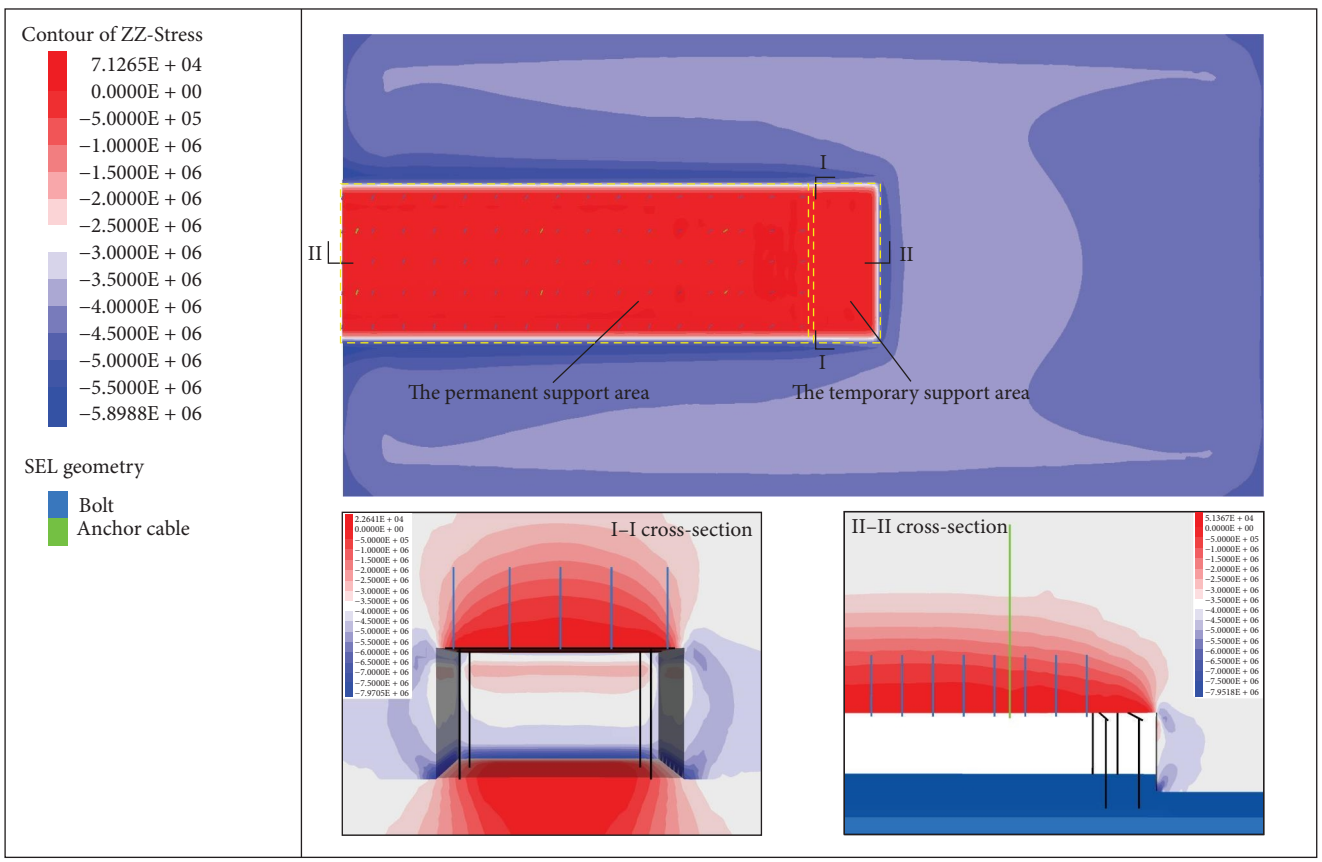

Figure 12: Vertical stress field cloud diagram.

unloading zone. At the end of the temporary support area, the vertical stress measures 7.1 MPa, with the roof's vertical stress being lower than that at the front end. This observation suggests that the surrounding rock of the heading structure and the anchorage support in the temporary support area possess a robust ability to withstand disturbances. However, the middle section of the temporary support area's roof relies solely on the strength of the rock mass itself and the temporary support components to resist disturbances. Consequently, when the distance to the roof is 3.4 m, the deformation of the surrounding rock within the temporary support area remains minimal, indicating favorable stability.

Figure 13 illustrates the cloud map of the vertical displacement distribution of the surrounding rock in the temporary support area tailgate. The figure reveals a U-shaped ring distribution of the vertical displacement of the tailgate roof in the temporary support area along the vertical profile. The vertical displacement progressively increases from the surrounding area towards the center, and the region of vertical displacement development shifts with the distance from

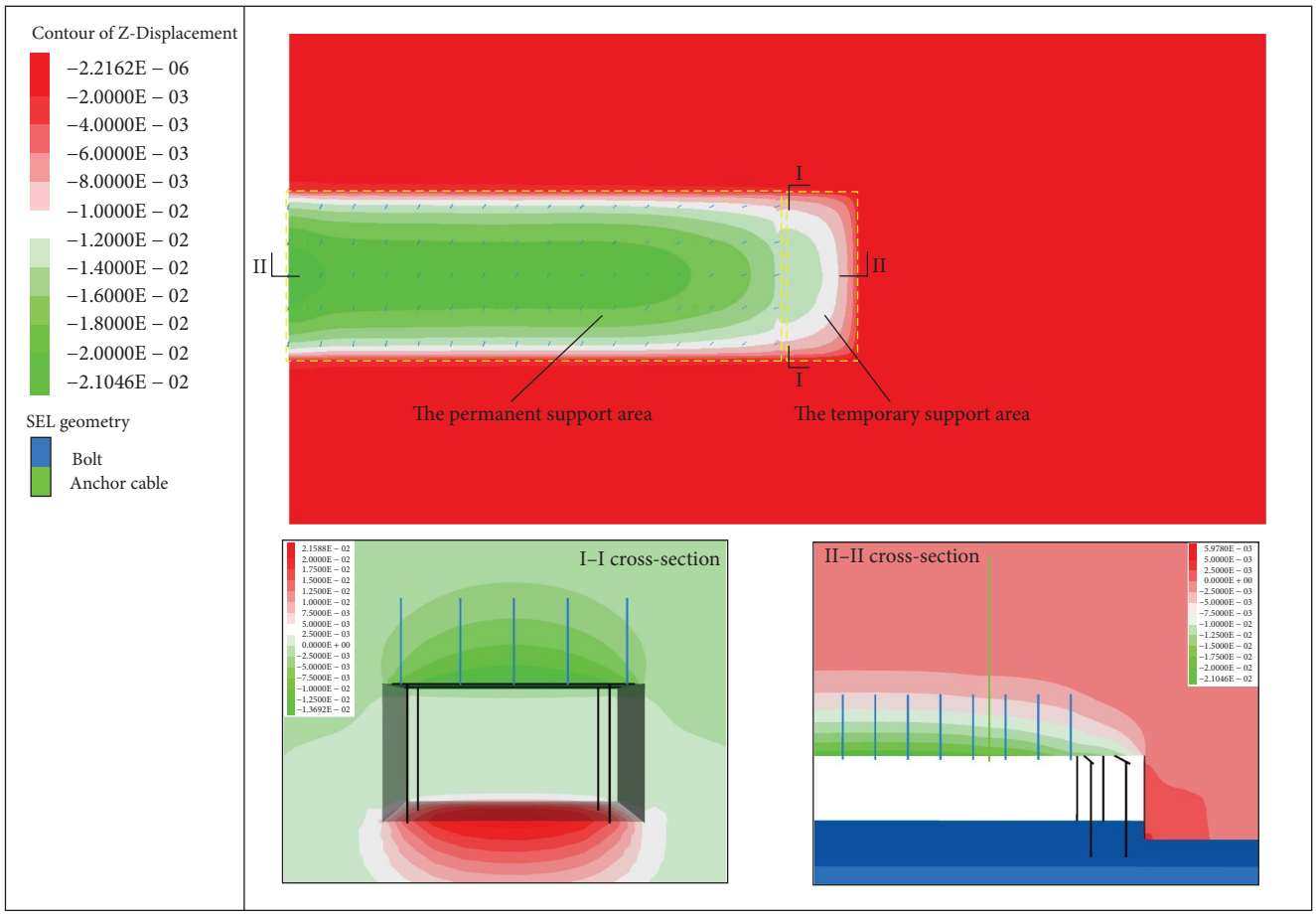

Figure 13: Vertical displacement field cloud diagram.

the support area. The maximum displacement of the tailgate roof measures 0.021 m, indicating effective control of the surrounding rock in the tailgate.

Through the analysis of stress and displacement in the temporary support area of the roadway, it can be concluded that the maximum stress and deformation occur at the midpoint of the temporary support area. Figure 14 illustrates the distribution of the plastic zone in the temporary support area. The plastic zone extends further in the rib angle compared to the coal body section, indicating a larger evolution range. The roadway experiences both shear and tensile forces, leading to the formation of cracks within the rock mass in the plastic zone. The disturbance range of the surrounding rock is relatively small, while the plastic zone in the middle of the roof of the roadway reaches a maximum height of 0.9 m.

5.5. Application Effect Evaluation. For the purpose of assessing the stability of the surrounding rock in the roadway. A 300 m section in the tailgate of the 30304 panel was selected for field testing, and the monitoring of surface displacement in the roadway was conducted over a period of 28 days. The resulting deformation curve of the surrounding rock is depicted in Figure 15. Based on the monitoring data, it is evident that the deformation of the surrounding rock can be categorized into three distinct stages.

(1) Stage I takes place within 0–4 days after roadway excavation, during which the roadway experiences rapid deformation. The rate of deformation is significantly higher for the roof and floor and the two sides, with maximum migration rates of 11.8 and 4.12 mm/day.

(2) Stage II occurs 4–12 days after roadway excavation and is characterized by a gradual decrease in deformation rate. During this stage, the surrounding rock gradually couples with the supporting structure, leading to a reduced rate of deformation in the roof, floor, and sidewalls.

(3) Stage III, which occurs after 12 days, represents a stable development phase in the mining process. During this stage, the average rate of roof and floor movement ranges from 0.1 to 1.7 mm/day, while the deformation rate of the two sides ranges from 0.01 to 0.04 mm/day. Once stabilized, the displacement of the roof and floor measures 24.0 mm, while the two sides experience a displacement of 8.99 mm. The study employed an effective support form, which successfully controlled the separation and failure deformation of the roadway, resulting in a significant improvement in the internal stability of the surrounding rock.

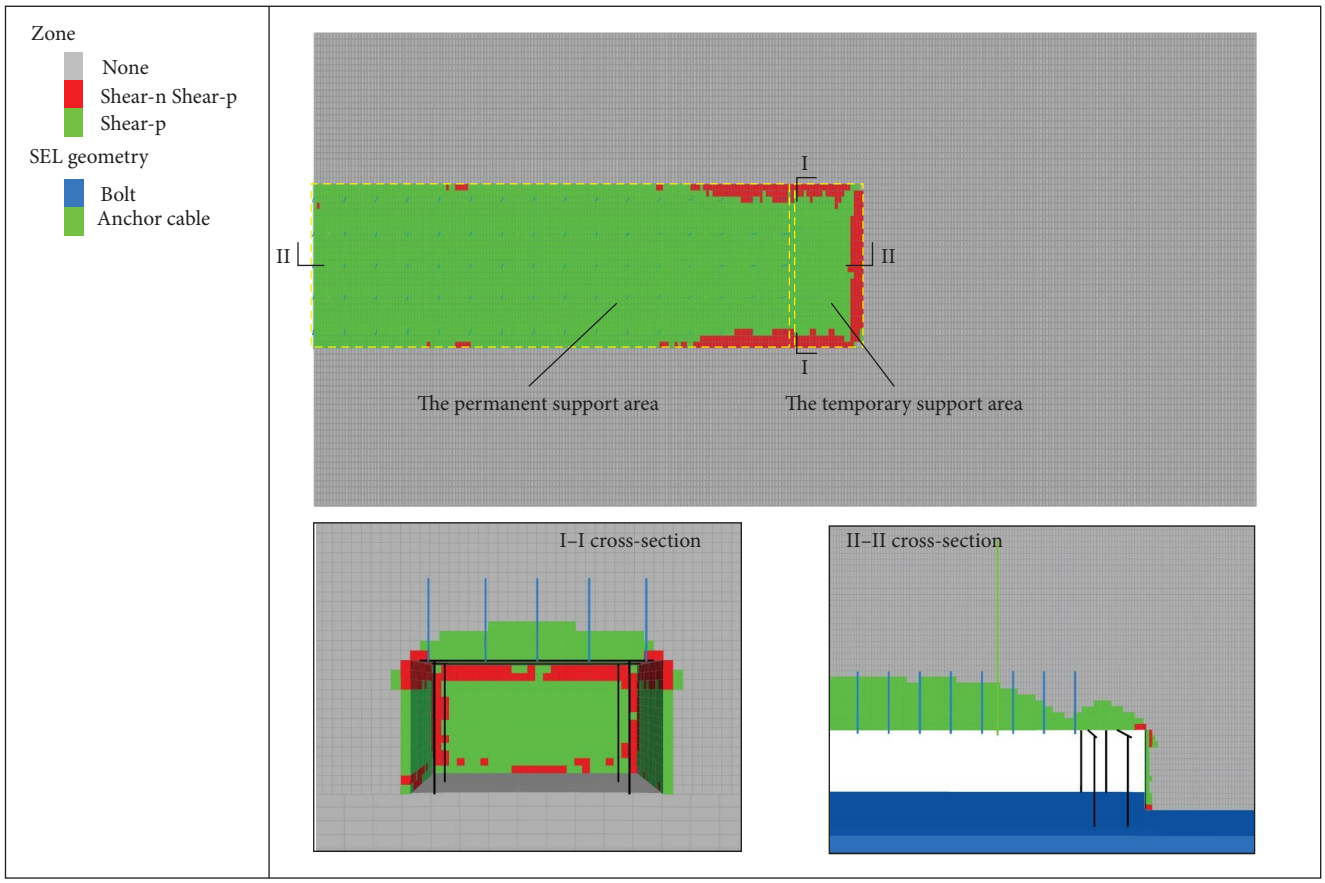

Figure 14: Distribution diagram of plastic zone.

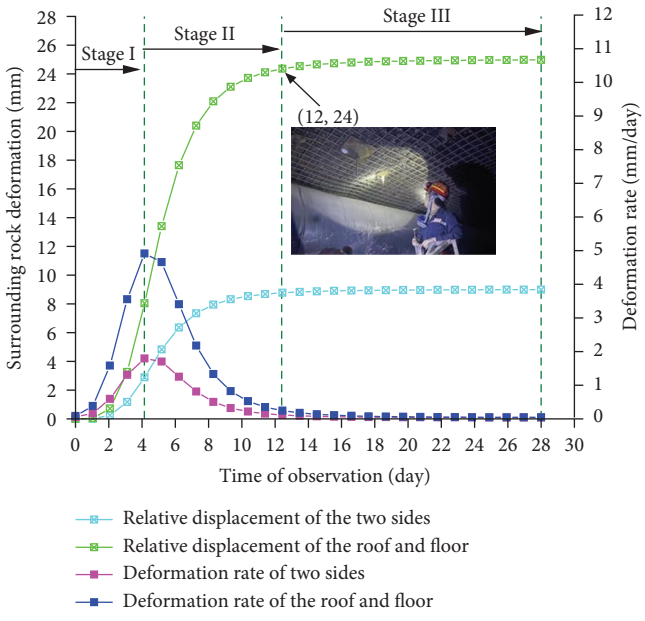

Figure 15: Deformation curve of roadway.

6. Conclusion

(1) By considering the stress state of the surrounding rock at the excavation face, a mechanical model is established to analyze the roof in the excavation face area. Utilizing the principle of the superposition method in material mechanics, an equation for the deflection curve of the immediate roof in the temporary support area is derived.

(2) The derived deflection curve equation is used to calculate the maximum unsupported roof distance of the heading face. Additionally, the calculation method for key parameters in this formula is obtained. A comparative analysis is conducted between this formula and the existing calculation formula for the maximum unsupported roof distance of the "plate" model. The applicability conditions of both formulas are analyzed.

(3) The deformation of the roof in the temporary support area of the excavation face is influenced by ten factors. Through single-variable sensitivity analysis, it has been determined that the thickness of the immediate roof (h_m), the distance from the peak of the abutment pressure to the coal wall (L_3), and the length of the temporary support area (L_1) are the key influencing factors. The deformation pattern of the roof is analyzed when there is a bivariate interaction between the support load and the length of the temporary support area.

(4) Based on the engineering background of the Yanghuopan Coal Mine, it has been calculated that the

maximum unsupported roof length of the 30304 tailgate is 3.4 m. The results of numerical simulation and field monitoring indicate that the deformation of the roof in the excavation face is relatively small, and the stability of the surrounding rock mass is good.

Data Availability

The data used to support the findings of this study are included in the article.

Conflicts of Interest

The authors declare that they have no conflicts of interest.

Acknowledgments

Thanks to Shoushi Gao, Yifeng He, and Tao Yang for their technical help in collaborating on the experimental work. I would also like to thank Bing Wang, Li Wang, Haibo Pang, and Bing Peng for providing helpful inspiration, suggestions, guidance, review, and supporting work. This research was funded by the National Natural Science Foundation of China (nos. 51774229 and 52004200).

References

[1] H. P. Kang, "Seventy years development and prospects of strata control technologies for coal mine roadways in China," *Chinese Journal of Rock Mechanics and Engineering*, vol. 40, no. 1, pp. 1–30, 2021.

[2] Y. Chen, J. B. Bai, S. Yan, S. P. Hao, and V. D. Dao, "A method for computing unsupported roof distance in roadway advancement and its in-situ application," *International Journal of Mining Science and Technology*, vol. 26, no. 4, pp. 551–556, 2016.

[3] J. B. Bai, T. Q. Xiao, and L. Li, "Unsupported roof distance determination of roadway excavation using difference method and its application," *Journal of China Coal Society*, vol. 36, no. 6, pp. 920–924, 2011.

[4] N. Zhang, C. L. Han, and Z. Z. Xie, "Theory of continuous beam control and high efficiency supporting technology in coal roadway," *Journal of Mining and Strata Control Engineering*, vol. 1, no. 2, pp. 48–55, 2019.

[5] Z. W. Ding, X. F. Li, J. Zhang et al., "A theoretical analysis of unsupported roof plate and shell in excavation roadway and numerical calculation and verification of transcendental function," *Journal of Mining and Safety Engineering*, vol. 38, no. 3, pp. 507–517, 2021.

[6] M. Shabanimashcool and C. C. Li, "Analytical approaches for studying the stability of laminated roof strata," *International Journal of Rock Mechanics and Mining Sciences*, vol. 79, pp. 99–108, 2015.

[7] H. B. Yang, S. M. Li, B. L. Fang et al., "Study on structural instability of roadway surrounding rock based on elastic hole theory," *Safety in Coal Mines*, vol. 50, no. 6, pp. 254–257, 2019.

[8] M. Fraldi and F. Guarracino, "Limit analysis of collapse mechanisms in cavities and tunnels according to the Hoek–Brown failure criterion," *International Journal of Rock Mechanics and Mining Sciences*, vol. 46, no. 4, pp. 665–673, 2009.

[9] X. Zhang, M. N. Wang, J. W. Li, Z. L. Wang, J. J. Tong, and D. G. Liu, "Safety factor analysis of a tunnel face with an unsupported span in cohesive-frictional soils," *Computers and Geotechnics*, vol. 117, Article ID 103221, 2020.

[10] J. H. Yang, Z. S. Jiang, and S. R. Xie, "Stability analysis and control technology of surrounding rocks at deep large cross-section roadway," *Coal Science and Technology*, vol. 48, no. 6, pp. 49–56, 2020.

[11] W. T. Tang, S. Y. Li, W. Liu, and Z. F. Wang, "Study on unsupported roof distance of roadway driving with broken roof," *Safety in Coal Mines*, vol. 44, no. 10, pp. 38–40 44, 2013.

[12] Z. Y. Xia and Z. Y. Tan, "Study on instability mechanism of extraction structure under undercut space based on thin plate theory in block caving method," *Shock and Vibration*, vol. 2021, no. 2, Article ID 5548213, 11 pages, 2021.

[13] S. C. Tian, X. L. Xu, and Z. L. Li, "Disaster-inducing mechanism in a roadway roof near the driving face and its safety-control criteria," *Safety Science*, vol. 115, pp. 208–214, 2019.

[14] S. Yang, N. Zhang, X. W. Feng, D. J. Pang, and D. Y. Qian, "The influence of heading rate on roof stability in coal entry excavation," *Advances in Civil Engineering*, vol. 2018, Article ID 9841374, 15 pages, 2018.

[15] X. Liu, X. Z. Hua, P. Yang, and Z. G. Huang, "A study of the mechanical structure of the direct roof during the whole process of non-pillar gob-side entry retaining by roof cutting," *Energy Exploration & Exploitation*, vol. 38, no. 5, pp. 1706–1724, 2020.

[16] S. Q. Yang, M. Chen, H. W. Jing, K. F. Chen, and B. Meng, "A case study on large deformation failure mechanism of deep soft rock roadway in Xin'An coal mine," *Engineering Geology*, vol. 217, pp. 89–101, 2017.

[17] H. S. Jia, K. Pan, S. W. Liu et al., "The deformation and failure mechanism and control technology of mining influenced roadway sides," *Journal of Mining and Safety Engineering*, vol. 37, no. 4, pp. 689–697, 2020.

[18] L. C. E. F. Filho, M. E. Hartwig, and C. A. Moreira, "EPB excavation in transitional mixed face: Line 5—Lilac (São Paulo Metro, Brazil)," *Bulletin of Engineering Geology and the Environment*, vol. 81, no. 5, 2022.

[19] J. K. Meng, T. Q. Xiao, and S. Y. Jiang, "Supporting technology speedy drivage roadway in shoushan no. 1 coal mine," *Safety in Coal Mines*, vol. 46, no. 1, pp. 122–125, 2015.

[20] G. X. Xie, C. M. Li, and L. Wang, "Mechanical characteristics and practical application on stress shell of road way surrounding rock," *Journal of China coal society*, vol. 41, no. 12, pp. 2986–2992, 2016.

[21] Y. Z. Hernandez, A. D. Farfan, and A. P. de Assis, "Three-dimensional analysis of excavation face stability of shallow tunnels," *Tunnelling and Underground Space Technology*, vol. 92, Article ID 103062, 2019.

[22] P. T. Simic-Silva, B. Martínez-Bacas, R. Galindo-Aires, and D. Simic, "3D simulation for tunnelling effects on existing piles," *Computers and Geotechnics*, vol. 124, Article ID 103625, 2020.

[23] J. Li, *Research on the Technology of Long Distance Temporary Support in the Heading Face of Semi-Coal Rock Roadway in Dangjiahe Mine*, Henan Polytechnic University, China, 2020.

[24] F. Luo, S. G. Cao, G. D. Li, Y. Li, and P. Guo, "Evolution characteristics of fracture and instability in coal roadways and subregional supporting," *Journal of Mining and Safety Engineering*, vol. 34, no. 3, pp. 479–487, 2017.

[25] S. Yang, X. Z. Hua, X. Liu, and C. Li, "Analysis of stability factors of roadway roof and determination of unsupported roof distance," *Shock and Vibration*, vol. 2021, Article ID 2271257, 13 pages, 2021.
[26] J. C. Cao, N. Zhang, S. Y. Wang, D. Y. Qian, and Z. Z. Xie, "Physical model test study on support of super prestressed anchor in the mining engineering," *Engineering Failure Analysis*, vol. 118, Article ID 104833, 2020.
[27] H. M. Liu, X. L. Li, and Z. Y. Yu, "Influence of hole diameter on mechanical properties and stability of granite rock surrounding tunnels," *Physics of Fluids*, vol. 35, no. 6, 2023.
[28] H. T. Li, X. L. Li, J. H. Fu et al., "Experimental study on compressive behavior and failure characteristics of imitation steel fiber concrete under uniaxial load," *Construction and Building Materials*, vol. 399, Article ID 132599, 2023.
[29] D. W. Yin, S. J. Chen, Y. Ge, and R. Liu, "Mechanical properties of rock–coal bi-material samples with different lithologies under uniaxial loading," *Journal of Materials Research and Technology*, vol. 10, no. 1–4, pp. 322–338, 2021.
[30] S. J. Chen, J. C. Zhang, D. W. Yin, F. X. Li, J. L. Lu, and P. Y. Zhu, "Visualizing experimental investigation on gas–liquid replacements in a microcleat model using the reconstruction method," *Deep Underground Science and Engineering*, pp. 1–9, 2023.
[31] T. S. Dang, N. Wessels, N.-S. Nguyen, K. Hackl, and G. Meschke, "A coupled computational approach for the simulation of soil excavation and transport in earth-pressure balance shield machines," *International Journal for Multiscale Computational Engineering*, vol. 15, no. 3, pp. 239–264, 2017.
[32] Z. B. Zhang, E. Y. Wang, N. Li, H. T. Zhang, Z. M. Bai, and Y. H. Zhang, "Research on macroscopic mechanical properties and microscopic evolution characteristic of sandstone in thermal environment," *Construction and Building Materials*, vol. 366, Article ID 130152, 2023.
[33] Z. B. Zhang, E. Y. Wang, H. T. Zhang, Z. M. Bai, Y. H. Zhang, and X. U. Chen, "Research on nonlinear variation of elastic wave velocity dispersion characteristic in limestone dynamic fracture process," *Fractals*, vol. 31, no. 1, 2023.